EM-ICP strategies for joint mean shape and correspondences estimation: applications to statistical analysis of shape and of asymmetry

Benoît Combès, Marc Fournier, David N. Kennedy, José Braga, Neil Roberts, Sylvain Prima

EM-ICP STRATEGIES FOR JOINT MEAN SHAPE AND CORRESPONDENCES ESTIMATION: APPLICATIONS TO STATISTICAL ANALYSIS OF SHAPE AND OF ASYMMETRY

Benoît Combès[1], Marc Fournier[1], David N. Kennedy[2], José Braga[3], Neil Roberts[4] and Sylvain Prima[1]

[1] INSERM, U746, Faculté de Médecine CS 34317, INRIA, VisAGeS, Univ. Rennes I, CNRS, UMR 6074, IRISA, Rennes, France

[2] Division of Neuroinformatics, Department of Psychiatry, University of Massachusetts Medical School

[3] AMIS, Paul Sabatier University, Toulouse, France

[4] CRIC, Queen's Medical Research Institute, Edinburgh, U.K.

ABSTRACT

In this paper, we propose a new approach to compute the mean shape of unstructured, unlabelled point sets with an arbitrary number of points. This approach can be seen as an extension of the EM-ICP algorithm, where the fuzzy correspondences between each point set and the mean shape, the optimal non-linear transformations superposing them, and the mean shape itself, are iteratively estimated. Once the mean shape is computed, one can study the variability around this mean shape (e.g. using PCA) or perform statistical analysis of local anatomical characteristics (e.g. cortical thickness, asymmetry, curvature). To illustrate our method, we perform statistical shape analysis on human osseous labyrinths and statistical analysis of global cortical asymmetry on control subjects and subjects with situs inversus.

***Index Terms*—** point set, mean shape, EM-ICP, shape analysis, symmetry, surface

1. INTRODUCTION

Algorithmic tools for groupwise anatomical studies are of great interest to characterise and compare anatomical structures over and between populations in an efficient and comprehensive way. Lots of efforts have been made to design methods allowing to build statistical shape models (*i.e.* defining and computing a mean shape M from the observations and characterising the main variations of the shapes around M) when the shapes are represented by implicit surfaces, meshes or simple point sets. Recent works include methods based on i) the minimum description length (MDL) theory [1]: one looks for the most compact model (*i.e.* involving as few parameters as possible) that best explains the population or on ii) the definition of the mean shape as the minimiser of a registration-like criterion [2, 3, 4, 5, 6]; the subsequent model simply explains the variability of the population with respect to the distance (typically a mixture of data superimposition distance and of smoothness of the underlying transformations) assumed by the registration criterion.

Among this last class of methods, the Mean Shape EM-ICP (MS-EM-ICP) recently developed by Hufnagel and colleagues [4] is based on the original EM-ICP developed by Granger and Pennec [7] and more recently extended to handle non-linear deformations efficiently [8]. This algorithm relies on a probabilistic modelling of the point-to-point correspondences that allows i) a pragmatic definition of the superimposition of two point sets and ii) to work on a relatively smooth cost function to minimise [7]. Moreover, this approach is well-grounded (monotonic convergence), generic (no assumption on tessellation/topology/number of points), can deal with large point sets and can be easily improved in many ways (adding priors, ...). However, only a few works have been dedicated to the investigation of the ability to this approach to perform groupwise studies.

The purpose of this paper is to extend the previous work of Hufnagel and colleagues and show that the EM-ICP approach leads to particularly simple and powerful solutions for groupwise studies. In particular, its underlying probabilistic modelling allows to define the mean shape of a given population and the projection of individual pointwise information on the mean shape in a simple way. In Section 2, we first introduce the mean shape EM-ICP (MS-EM-ICP) algorithm as an extension of the classical Procrustean mean to unlabelled point sets. From a population of point sets $X = \{X^1, \ldots, X^C\}$, the MS-EM-ICP allows to estimate both a mean shape M and a "virtual" correspondent of each point of M in each point set X^c. Then we identify some flaws of the MS-EM-ICP and develop two alternative extensions of the MS-EM-ICP allowing to tackle them. Finally, we show that these algorithms allow to perform statistical shape analysis (*e.g.* PCA) and to project individual local characteristics (*e.g.* cortical thickness, asymmetry, curvature) on the common reference M. In Section 3, we show how the previous tools can be used to perform a statistical analysis of asymmetries over and between populations of anatomical structures. These tools entirely rely on extensions of the EM-ICP algorithm. Finally, we illustrate our methods on real applications for the shape analysis of osseous labyrinths (Section 4.2) and the comparison global of cortical asymmetry between two patients with situs inversus and a control population (Section 4.3).

2. MEAN SHAPE AND VIRTUAL CORRESPONDENCES TO THE MEAN SHAPE

In this section, we first present the mean shape EM-ICP (MS-EM-ICP) algorithm (Section 2.1.2) as an extension of the Procrustean mean to unlabelled point sets (Section 2.1.1). Then, we study its limitations (Section 2.1.3) and we propose two extensions aiming at tackling these limitations (Section 2.2.1 and Section 2.2.2). Finally, we notice that the MS-EM-ICP algorithm outputs some quantities allowing to compute virtual correspondences from each X^c to M and to project efficiently pointwise information of each X^c to M (Section 2.3).

2.1. Mean shape EM-ICP

2.1.1. Basics: labelled point sets

The Procrustean mean is a Fréchet mean for the space of labelled point sets. This space is defined as the orbit space of the non-coincident point set configurations under the action of the rigid-body (or similarity) transformation. In other words, the shape of an object is defined as the geometrical information that remains when one filters out translation, rotation (and optionally scale). The distance from a shape $V^1 = \{v_1^1, \ldots, v_N^1\}$ to another shape $V^2 = \{v_1^2, \ldots, v_N^2\}$ is considered as the sum of the squared Euclidean distances between each labelled point after an optimal rigid (or rigid plus scale) alignment of the shapes. In case of rigid-body alignment, this Procrustean distance writes:

$$d^2(V^1, V^2) = \min_T \sum_i ||T(v_i^1) - v_i^2||^2, \tag{1}$$

where T is a rigid-body transformation. This distance d allows the definition of the Fréchet mean for d of a set of labelled point sets $V = \{V^1, \ldots, V^C\}$:

$$\tilde{M} = \arg\min_M \sum_{c=1}^{C} d^2(M, V^c). \tag{2}$$

$\tilde{M}$ can be computed using the classical Procrustean superimposition framework:

Init: choose an arbitrary reference point set V^{ref} in V
Step 1: compute the optimal rigid body transformation $\tilde{T}^c$
for all c, $\tilde{T}^c = \arg\min_{T^c} \sum_i ||T^c(v_i^c) - v_i^{ref}||^2$
Step 2: compute the optimal mean shape $\tilde{M}$
for all i, $\tilde{m}_i = \frac{1}{C} \sum_c \tilde{T}^c(v_i^c)$

Then the variability of the population around the mean can be studied by analysing the residuals $(V^c - M)$ (*e.g.* using PCA).

2.1.2. Basics : unlabelled point sets

However, in practice, defining and labelling adequate points (landmarks) characterising the surfaces of interest is often problematic. To cope with this limitation, one can study unlabelled point sets representing the surfaces under study. The classical Procrustean distance between two labelled point sets is what remains when the optimal superimposition has been applied, thus in order to extend this approach to unlabelled point sets, we have to design a measure of what remains when the optimal superimposition and the optimal labelling have been applied. The EM-ICP algorithm, designed as a solution to a ML problem for a rigid-body transform T superposing a point set $T(X^1)$ to its noised version X^2, is a pragmatic and efficient solution for this purpose. This ML estimation is performed by an EM algorithm that amounts to the alternated minimisation of the following criterion with respect to two unknowns T/A:

$$\delta^2(X^1, X^2) = \min_{A,T} \sum_{x_i^1 \in X^1} \sum_{x_j^2 \in X^2} A_{i,j} ||T(x_i^1) - x_j^2||^2 \tag{3}$$

$$+2\sigma^2 \sum_{i,j} A_{i,j} \log(A_{i,j}), \text{ with } \forall i,j, A_{i,j} \geq 0 \text{ and } \forall j, \sum_i A_{i,j} = 1$$

where:

- $A = (A_{i,j})$ is the match matrix encoding the *a posteriori* probabilities of correspondence between points of X^1 and of X^2. This probabilistic interpretation of A is linked to the presence of the barrier function $\sum_{i,j} A_{i,j} \log(A_{i,j})$ [3]. In essence, the greater $A_{i,j}$, the more likely the point $x_i^1 \in X^1$ to be the correspondent of the point $x_j^2 \in X^2$. σ^2 is the Gaussian noise variance on X. This fuzzy control on the correspondences allows to handle efficiently problems due to differences of sampling/number of points: we do not look for one-to-one correspondences between points of each shape but instead for "fuzzy" correspondences linking each point of X^2 to the surface represented by $T(X^1)$.
- T is a rigid-body (or rigid+scale) transformation superposing X^1 on X^2.

Strictly speaking, this departure δ is not a distance as it satisfies neither the symmetry constraint nor the triangle inequality. Note that the symmetry constraint could be achieved by symmetrising the criterion [8] but for a sake of clarity, we do not discuss this aspect here.

Then, if we consider a set of C unlabelled point sets (of different size) defining a population under study $X = \{X^1, \ldots, X^C\}$ and $\tilde{M} = \{m_1, ..., m_N\}$ as the mean shape corresponding to the population X (we consider the number of points N fixed), $\tilde{M}$ can be written as:

$$\tilde{M} = \arg\min_M \sum_{c=1}^{C} \delta^2(M, X^c) \tag{4}$$

$$\tilde{M} = \arg\min_M \sum_{c=1}^{C} \min_{A^c, T^c} \Big[\sum_{x_i^c \in X^c} \sum_{m_j \in M} A_{i,j}^c ||T^c(x_i^c) - m_j||^2 \tag{5}$$

$$+2\sigma^2 \sum_{x_i^c \in X^c, m_j \in M} A_{i,j}^c \log(A_{i,j}^c) \Big],$$

$$\text{with } \forall c, \forall j, \forall i A_{i,j}^c \geq 0, \text{ and } \forall c, \forall j, \sum_i A_{i,j}^c = 1,$$

where:

- for all c, $A^c = (A_{i,j}^c)$ is the match matrix linking X^c and M,
- T^c is either a rigid-body or a similarity transformation superposing X^c on M.

This formulation can be seen as an extension of the well-known EM-ICP algorithm [7] and can be viewed as a ML problem modelling $\tilde{M}$ as a noised version of $T^c(X^c)$ $(\forall c)$ that can be solved using an EM algorithm. This EM algorithm writes:

Algo MS1: MS-EM-ICP

Init: $\tilde{M}$ is one of the point sets from X. $\forall c$, $\tilde{T}^c = Id$
Step 1: update $\tilde{A}^c$
for all c, for all i, j, $\tilde{A}_{i,j}^c = \frac{\exp(-||\tilde{T}^c(x_i^c) - \tilde{m}_j||^2/(2\sigma^2))}{\sum_k \exp(-||\tilde{T}^c(x_k^c) - \tilde{m}_j||^2/(2\sigma^2))}$
Step 2: update $\tilde{T}^c$
for all c, $\tilde{T}^c = \arg\min_{T^c} \sum_i \sum_j \tilde{A}_{i,j}^c ||T^c(x_i^c) - \tilde{m}_j||^2$
Step 3: update $\tilde{M}$
for all j,$\tilde{m}_j = \frac{1}{C} \sum_c \sum_i \tilde{A}_{i,j}^c \tilde{T}^c(x_i^c)$

As for the original EM-ICP algorithm, this algorithm is iterative and decreases the value of the criterion (and increases the corresponding likelihood function) until local convergence.

$\tilde{M}$ is typically initialised using a point set from X that appears both of good quality (no hole, no segmentation artifacts) and a "typical" representative of X. Step 1 can be performed efficiently using a kd-tree. When T is a rigid/similarity transformation Step 2 has a closed-form solution. Step 3 is computationally tractable.

In this framework, one can interpret the mean shape as the one for which the sum of "fuzzy residuals" $\tilde{A}^c_{i,j}||\tilde{T}^c(x^c_i) - \tilde{m}_j||^2$ subject to optimal transformations $\tilde{T}^c$ and optimal match matrices $\tilde{A}^c$ is minimal. In this sense, it extends the classical Procrustean mean. Particularly, if we note $\tilde{v}^c_j = \sum_i \tilde{A}_{i,j}\tilde{T}^c(x^c_i)$ then $\tilde{m}_j = \frac{1}{C}\sum_c \tilde{v}^c_j$. We call $\tilde{v}^c_j$ the "virtual correspondent" of m_j in $\tilde{T}^c(X^c)$; the term "virtual" is coined because v^c_j is not guaranteed to be in $\tilde{T}^c(X^c)$. The algorithm MS1 can then be simply rewritten as:

Step 1: update correspondences $(\tilde{v}^c_j)$
for all c, compute $\tilde{T}^c$ and $\tilde{A}^c$
for all c, for all j, $\tilde{v}^c_j = \sum_i \tilde{A}_{i,j}\tilde{T}^c(x^c_i)$
Step 2: update $\tilde{M}$:
for each j, $\tilde{m}_j = \frac{1}{C}\sum_c \tilde{v}^c_j$

For a better understanding of this process, one can regard it as:

$$\tilde{M} = \arg\min_{M,V} \sum_c d^2(M, V^c(X^c, M)), \tag{6}$$

where M and $V^c(.,.)$ are labelled point sets with N points each and $d(.,.)$ is the Procrustean distance described in Eq. 1. Each labelled point set $V^c(X^c, M) = (\tilde{v}^c_j)$ ($c \in [1, \ldots, C]$) is obtained from the rigid (or rigid+scale) registration of X^c on M. Then the previous algorithm can be described as i) the estimation of V^c knowing the population X^c and M and ii) the estimation of M knowing V^c.

2.1.3. Limitations

This framework appears seductively simple: it naturally extends the classical Procrustes mean shape while solving the correspondence problem between the point sets under study, using all the points of the surfaces, in a unified probabilistic framework, where a well-defined likelihood criterion can be maximised using a 3-step iterative algorithm.

However, it is deceptively attractive and inherently flawed. In this framework, the point-to-point correspondences are computed based on the implicit hypothesis that the point sets are identical up to a rigid-body (or rigid+scale) transformation and a Gaussian noise. As a consequence, the further the shape of the surfaces are different from each other, the worse the correspondences. This is illustrated on Fig.1. In this case, the mean shape will then be computed based on erroneous matches, and the subsequent analysis of variability around this mean shape will be strongly biased. In other words, this algorithm turns out to be useless when there is a high variability within the set of point sets of interest.

To cope with this problem, following Hufnagel et al. [4], we could replace the rigid-body/similarity transformations by more general affine transformations. This improves the estimation of correspondences, but with the deleterious effect of removing the potentially relevant differences between the surfaces under study (such as non-uniform scaling or stretching).

In the following, we propose to explore this idea further by improving the previous definition of the mean shape by considering the transformations T^c ($c \in [1, \ldots, C]$) as non-linear transformations subject to regularisations $L(T^c)$. Interestingly, depending on the way we interpret the original MS-EM-ICP criterion, this improvement can lead to two different paradigms. These two paradigms are equivalent when T^c is a simple linear transformation but quite different when dealing with non-linear deformations. In the two following paragraphs, we discuss these two paradigms.

2.2. Handling non-linear transformations

2.2.1. First solution: adding penalised non-linear deformations in δ

The natural solution to handle non-linear transformations consists in replacing the linear transformation in Eq 3 by a non-linear transformation T subject to regularisation L:

$$\begin{aligned}\delta^2(X^1, X^2) = \min_{A^c, T^c} \sum_{x_i \in X^1} \sum_{x_j \in X^2} A_{i,j}||T(x^1_i) - x^2_j||^2 \\ + 2\sigma^2 \sum_{i,j} A_{i,j}\log(A_{i,j}) + \alpha L(T)\end{aligned} \tag{7}$$

where α weighs the strength of the regularisation over the data attachment term (including the barrier function $\sum_{i,j} A_{i,j}\log(A_{i,j})$). Roughly speaking, the subsequent mean shape $\tilde{M}$ is then defined as the shape that minimises both the overall "mismatches" $\sum_{x^c_i \in X^c}\sum_{m_j \in M} A^c_{i,j}||T^c(x^c_i) - m_j||^2$ and the deformation energies $\alpha L(T^c)$ between each X^c and $\tilde{M}$. The choice of the parameter α and of L is crucial as it has a strong impact on the definition of the mean shape and thus on the interpretation of the subsequent statistical model. Moreover, in order not to capture simple differences of pose, orientation (and optionally scale) of the point set X^c in the model, the regulariser L must not penalise rigid-body (or similarity) transformations.

Similarly to the original MS-EM-ICP, this modified criterion can be minimised by the following algorithm:

Algo MS2: non linear MS-EM-ICP

Step 1: update $\tilde{A}^c$
for all c, for all i, j, $\tilde{A}^c_{i,j} = \frac{\exp(-||\tilde{T}^c(x^c_i) - \tilde{m}_j||^2/(2\sigma^2))}{\sum_k \exp(-||\tilde{T}^c(x^c_k) - \tilde{m}_j||^2/(2\sigma^2))}$
Step 2: update $\tilde{T}^c$:
for all c, $\tilde{T}^c = \arg\min_{T^c} \sum_{i,j} \tilde{A}^c_{i,j}||T^c(x^c_i) - \tilde{m}_j||^2 + \alpha L(T^c)$
Step 3: update $\tilde{M}$:
for all j, $\tilde{m}_j = \frac{1}{C}\sum_c \sum_i \tilde{A}^c_{i,j}\tilde{T}^c(x^c_i)$

Step 1 can be performed efficiently using a kd-tree. Step 2 can be solved efficiently using the techniques we recently proposed in the registration context [8]. This algorithm is quite close to the one proposed by Chui and colleagues [3]. It mainly differs by the fact that Chui and colleagues introduce a clustering task in Step 1 allowing to reduce the size of matrices A^c and thus the computational burden during Step 2. We think that our solution is more natural and simpler than the one they propose.

2.2.2. Second solution: improving correspondence estimation using non linear deformations

Although the previous solution provides a first proposition, it importantly modifies the nature of the distance and thus the interpretation of the estimated mean with respect to the initial Procrustean point of view. Indeed, by modifying the deformation model as we did in Section 2.2.1, one both affects i) the estimation of correspondences and ii) the nature of the distance d considered as the sum of

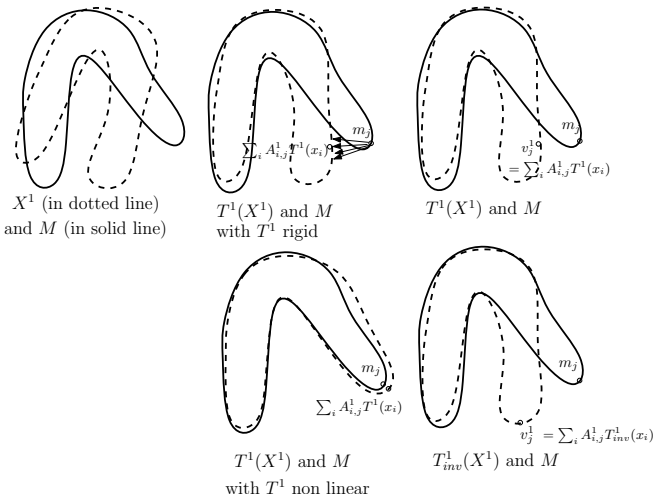

Fig. 1. **First row: Illustration of the classical MS-EM-ICP (MS1).** From left to right: i) the point set X^1 and M, ii) $T(X^1)$ and M (T^1 is a rigid-body transformation) and the resulting matching $\sum_i A^1_{i,j} T^1(x_i)$ and iii) the resulting correspondences $v^1_j = \sum_i A^1_{i,j} T^1(x_i)$, **Second row: Illustration of the improved MS-EM-ICP (MS3).** From left to right: i) $T^1(X^1)$ on M (T^1 is a non-linear smooth transformation) and the resulting matching $\sum_i A^1_{i,j} T^1(x_i)$ and ii) the resulting correspondences $v^1_j = \sum_i A^1_{i,j} T^1_{inv}(x_i)$.

"mismatches" $\sum_{x_i \in X^c} \sum_{m_j \in M} A^c_{i,j} ||T^c(x^c_i) - m_j||^2$ and of the deformation energies $\alpha L(T^c)$ between each X^c and $\tilde{M}$.

An alternative solution would consist in improving the estimation of the correspondences v^c_j by introducing a non-linear deformation linking M and X^c inside the criterion. However, to preserve the spirit of the original Procrustean mean, the non-linear deformations must affect only the estimation of the matrices A^c not to change the nature of the shape space (that is defined as an orbit space under the action of a simple rigid or similarity transformation). This view results in the following algorithm:

Algo MS3: Improved Procrustean mean on unlabelled point sets

Step 1: update correspondences ($\tilde{v}^c_j$):
$\forall c$, compute $\tilde{T}^c$ and $\tilde{A}^c$
$\forall c$, compute $\tilde{T}^c_{inv}$ as the rigid component of $\tilde{T}^c$
$\forall c, \forall j$, compute $\tilde{v}^c_j = \sum_i \tilde{A}^c_{i,j} \tilde{T}^c_{inv}(x^c_i)$
Step 2: update $\tilde{M}$:
for each j, $\tilde{m}_j = \frac{1}{C} \sum_c \tilde{v}^c_j$

Step 1 can be performed efficiently using the techniques proposed in [8]. Step 2 is computationally tractable. This algorithm can be seen as a generalisation of MS1 but we did not find any proper criterion it minimises. However, we observe that the value $\sum_c d(M, V^c(X, M))^2$ decreases throughout the iterations and that the obtained mean shape fits well the data X. An illustration of this strategy is given in the second row of Figure 1. By contrast with MS2, this algorithm provides a mean that does not depend directly on the regulariser L but on the quality of the correspondences obtained during the registration process. As a result, we think that this approach is less dependent on the design of L. On the other hand, by explicitly taking into account the regularisation into δ, MS2 is more suited to characterise large deformations linking a point set of the population X^c to the mean.

2.2.3. *Conclusion*

When modelling T^c as linear transformations (without penalisation), the two developed algorithms MS2 and MS3 are equivalent. When using non-linear transformations, the two algorithms describe two different points of view. As of now, we did not investigate the respective merits of both frameworks for the estimation of statistical model and in the following, we choose to use the improved automatic Procrustean mean (MS3) to perform mean shape estimation and statistical shape analysis because of i) its simplicity of interpretation as opposed to MS2 (largely depending on the choice of L/α) and ii) the easiness of the underlying statistical analysis (that can be performed from the virtual correspondence similarly to what is done in the classical Procrustean framework). Finally, notice that the estimations given by the algorithms MS1, MS2 and MS3 are initialisation dependent and thus provide biased means (contrary to the classical Procrustean mean for labelled point sets). The sensitivity to initialisation is a key property to investigate in future works.

2.3. Virtual correspondence & projection

As previously mentioned, the match matrices allow to compute the "virtual" correspondent of each point of the mean shape M to each point of the X^cs using the *a posteriori* probabilities of matching encoded in $A^c_{i,j}$ ($\forall c$): $v^c_j = \sum_i A^c_{i,j} T^c_{inv} x^c_i$. In the following, we assume that the point sets X^c are initially rigidly registered together and thus that $T_{inv} = Id$ and $v^c_j = \sum_i A^c_{i,j} x^c_i$.

Another interesting use of this *a posteriori* probability concerns the projection of pointwise individual mapping on the mean shape M. Consider that each point x^c_i of X^c contains a scalar information (*e.g.* cortical thickness, local asymmetry, curvature, ...) that we call $s^{X^c}_i$. Then, the projection of $S^{X^c} = (s^{X^c}_i)$ on M is given by $s^{X^c \to M}_j = \sum_i A^c_{i,j} s^{X^c}_i$. As $\forall j$, $\sum_i A^c_{i,j} = 1$, the "interpolated" value at m_j is a weighted mean of the values at different points of X^c. This last property will be useful below for the projection of individual asymmetry maps on a reference template.

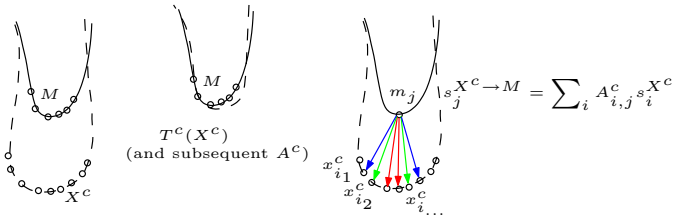

Fig. 2. **Projection of scalar information on the mean shape:** From left to right i) mean shape M and X^c. ii) M and $T^c(X^c)$ (computed jointly with M). iii) the subsequent correspondences (hot (resp. cold) colors indicate high (resp. low) values for $A^c_{i,j}$) between each point m_j and points of X^c allow to compute the projected scalar information at point m_j of M.

3. QUANTIFICATION OF ASYMMETRIES OVER/BETWEEN POPULATIONS

In this section, based on the previously described tools, we develop a pipeline for the quantification of asymmetries over or between populations. We consider that all the structures can be and are oriented

in a common orthogonal frame consisting of three axes that we call anterior-posterior, left-right and head-foot.

3.1. Computation of individual asymmetry maps

Let $X^c \in X$ be a point set representing an anatomical structure under study. Its *individual asymmetry maps* are computed as follows:

1. computation of the *approximate symmetry plane* P of X^c using a modified EM-ICP algorithm [9].
2. computation of the *asymmetry field* as the deformation field best superposing X^c and $S_P(X^c)$ using another modified EM-ICP algorithm [8].
3. computation of the 3 *individual asymmetry maps* by projecting each pointwise vector of the asymmetry field on the 3 coordinate axes. This allows to differentiate the anterior-posterior, left-right and head-foot components of the asymmetry field. This leads to 3 different scalar *asymmetry maps* for each point set X^c. We call these asymmetry maps $S^{X^c,AP}$, $S^{X^c,LR}$ and $S^{X^c,HF}$.

3.2. Computation of a mean shape & projection of the asymmetry mappings

We consider C point sets $X^1, \ldots, X^C$ representing the C structures under study. Their individual asymmetry maps $S^{X^c,AP}$ $S^{X^c,LR}$ and $S^{X^c,HF}$ have to be put in a common geometry to be compared. For this purpose, we use the algorithm MS3 described above to iteratively compute:

1. the point set M representing the mean shape,
2. the match matrices $\{A^1, \ldots, A^C\}$ (describing the fuzzy point-to-point correspondences between the point sets X^c and M),
3. the transformations T^c (best superposing the point sets X^c and M).

Once the mean point set M and the fuzzy match matrices A^C are computed, we project each individual (scalar) asymmetry maps $S^{X^c,AP}$, $S^{X^c,LR}$ and $S^{X^c,HF}$ on M which provides the *normalised individual asymmetry maps* $S^{X_i \to AP}$, $S^{X_i \to M,LR}$ and $S^{X_i \to M,HF}$. As pointed out in Section 2.3, the mapping at point $m_j \in M$ is defined as $s_j^{X^c \to M,AP} = \sum_i A_{ij}^c s_i^{X^c,AP}$ (and similarly for $s^{X^c \to M,LR}$ and $s^{X^c \to M,HF}$).

4. EXAMPLES OF APPLICATION

4.1. Implementation details

The transformation T is parametrised as a deformation field (*i.e.* $T(x) = x + t(x)$). The regularisation $L(T) = L(t)$ is chosen as a scalar Fourier based regulariser:

$$L(t = (t_1, t_2, t_3)^T) = L(t_1) + L(t_2) + L(f_3),$$

$$\text{with } L(t_i) = \frac{1}{(2\pi)^3} \int_{-\infty}^{\infty} \frac{|t_i^*(\omega)|^2}{\phi^*(|\omega|/b)} d\omega,$$

where * is the Fourier transform operator, $\phi : \mathbb{R} \to \mathbb{R}$ is an integrable function and b is a real positive rescaling factor. We choose ϕ as a Wu kernel. The resulting algorithmic solutions are given in a previous work [8].

The parameters are initialised as: $\alpha = 400$, $\sigma^2 = 20 \times S$, $b = 250 \times S$ where S is the size (in metres) of the object; α, σ^2, b are then decreased throughout the algorithm until they reach the respective values of 20, $5 \times S$ and $150 \times S$.

Finally, notice that we add a second match matrix B that is column stochastic in addition to the first match matrix A that is row stochastic in the function δ (Eq. 3 and 7). This modification does not change the general minimisation strategy and tends to make the formulation of δ more symmetrical (particularly the matching process) and to improve the estimation of correspondences between points. We omitted these details in the previous sections for a sake of clarity.

4.2. Shape analysis on osseous labyrinths

The shape analysis of the inner ear, and especially of the vestibular system (composed of the three semicircular canals) could be relevant to understand diseases such as adolescent idiopathic scoliosis, which affects about 3% of children between 10 and 16 worldwide [10]. More generally, the morphometric analysis of the bony/osseous labyrinth (that houses the membranous semicircular canals, the vestibule and the cochlea) has been shown to be key to the establishment of phylogenetic affinities between fossil hominids [11].

We segmented 15 osseous labyrinths of modern *Homo sapiens* from CT images with `amira.com`, giving surfaces of about 30,000 points. We validated our non-linear registration method on osseous labyrinths in a previous paper [8]. In Fig 3, we display the mean and two principal modes of variations around the mean obtained by analysing these 15 osseous labyrinths using MS3 and a principal component analysis on the residuals $(M - V^c)$ (where V^c are the virtual correspondents of M with respect to point set X^c). These results illustrate the ability of our algorithm to work on large and very convoluted structures with complicated topologies.

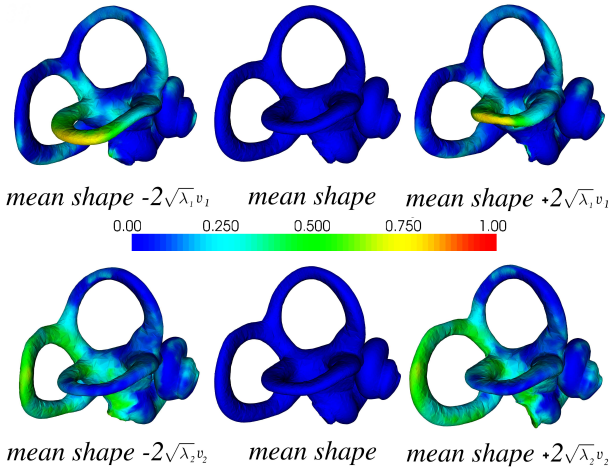

Fig. 3. **Mean shape and first modes of variation on 15 osseous labyrinths.** The magnitude of the deformations around the mean are mapped. The first mode of variation can be mainly interpreted as a change of size and of position of the lateral semicircular canal. The second mode of variation can be mainly interpreted as a change of size of the posterior semicircular canal.

4.3. Global cerebral asymmetries of subjects with situs inversus

Subjects with situs inversus (SI) have the potential to provide unique clues into the developmental mechanisms underlying the brain anatomical asymmetry and its relationship with hemispheric dominance for language. Situs inversus is a very rare condition where all the visceral organs are on the opposite side of the body to where they would be expected and as if they were reflected in a mirror.

Indeed, Kennedy [12] *et al.* report that the brain torque (reversed left-right differences in position and width of the frontal and occipital lobes) is reversed in subjects with situs inversus and that leftward anatomical asymmetry of language structures *e.g.* planum temporale is present in situs inversus. Moreover, Kennedy *et al.* suggest a left hemisphere functional dominance for language using fMRI [12]. Therefore, structurally there seems to be preserved local asymmetries of language-related structures in situs inversus but reversed torque and reversed functional dominance for language.

4.3.1. Material

Subjects: Data were available for two right-handed male subjects with situs inversus [12]. Both were aged 33 years. The control subjects are eleven right-handed male volunteers, ranging in age from 24 to 42 years (mean 28 $\pm$ 4.8).

Preprocessing: For each subject's MRI, the following pipeline was applied. We first segmented grey matter and separated each hemisphere (`surfer.nmr.mgh.harvard.edu`). The mesh was smoothed to remove inter-subject variability arising from the gyri and sulci using a technique similar to the one proposed in [13]. By removing the gyri and the sulci, we concentrate our study on gross brain asymmetries. Each generated mesh contains about 100K points.

4.3.2. Results

Pointwise results: We computed the collection of C ($\times$ 3) scalar normalised individual asymmetry maps $S^{X_1 \to M}, \ldots, S^{X_C \to M}$ projected on a common mean mesh M. For each point of M and each of the 3 components of the asymmetry field, we computed the mean asymmetry and its standard deviation over the 11 subjects and we performed a pointwise t-test with the null hypothesis H_0: "There is a perfect symmetry". We corrected the obtained p-values for multiple comparisons using permutation tests. Then, we compared the control and the SI populations by performing a pointwise permutation test (H_0: both SI subjects belong to the control population) using the mean difference as a statistic (correcting p-values for multiple comparisons). In Figures 4 and 6, we display components of the asymmetry field and views that appear the most significant. In Figure 5, we display the asymmetry maps for one of the two SI patients.

Integrated results: For an easier interpretation of the results, we integrated the pointwise asymmetry values over the frontal and occipital lobes of each of the subjects. Both lobes were extracted following affine registration of the LONI LPBS40/SPM5 atlas [14] to each subject of each of the subjects. Then for each subject, we computed the average left-right ("width") and the posterior-anterior ("protrusion") components for both the frontal (F) and occipital (O) lobes. To be even more synthetic, for each subject we noted the lobe (L or R, *i.e.* left or right) that appears *wider* and that *protrudes more* than its counterpart. When the difference in width or protrusion between the hemispheres was low ($< 10^{-1}$ mm), we noted 0 instead of L or R. For both the width (L-R), protrusion (P-A) components of the asymmetry field over the frontal and occipital lobes), we performed a t-test with the null hypothesis H_0: "There is a perfect symmetry". This integrated analysis was performed both on controls and SI subjects (Table 1 and Table 2).

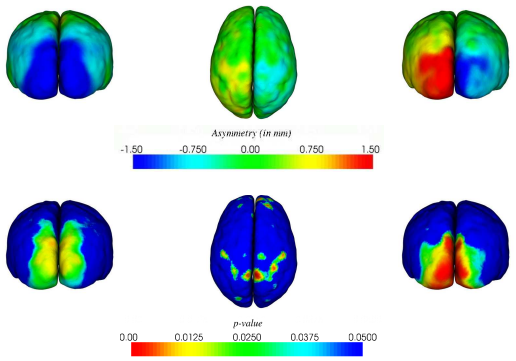

Fig. 4. **Mean (first row) and p-value (second row) for each of the 3 components of the asymmetry field (11 subjects)**. From left to right: left-right, head-foot, posterior-anterior components of the asymmetry field. Only the most significant view for each of the 3 tests is displayed (From left to right; posterior, above and posterior)

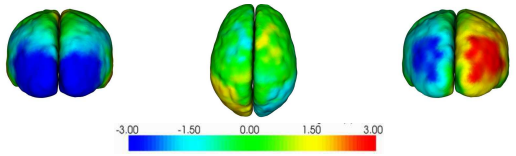

Fig. 5. **Asymmetry maps obtained for one of the SI subject**. We display the same views and the same components as in Figure 4. From left to right: left-right, head-foot, posterior-anterior components of the asymmetry field.

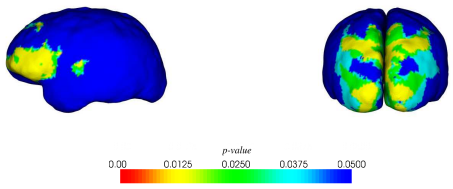

Fig. 6. **p-value of permutation test with H_0: SI population and control population are identical** From left to right: left-right and posterior-anterior components of the asymmetry field.

4.3.3. Interpretation

Control population: At the population level, and at the chosen significance level (p=0.05, corrected for multiple comparisons) the left occipital lobe appears to be wider (or bending towards the other side) and protrudes more posteriously than the right occipital lobe (Fig. 4 and Table 1). This observation is in line with the literature. At last and interestingly, we also find an area in the parietal lobe with a small significant "vertical" (head-foot) asymmetry: the right side seems to be "higher" compared to its counterpart (Fig. 4).

	1	2	3	4	5	6	7	8	9	10	11	p
O protrusion	L	L	L	L	R	L	L	L	L	L	0	p<0.05
O width	L	L	0	L	R	L	L	L	L	L	L	p<0.05
F protrusion	R	R	R	R	L	R	L	R	L	L	0	p>0.05
F width	R	L	0	R	R	0	L	0	L	R	L	p>0.05

Table 1. **Protrusion/width interhemispheric differences.** We display these differences for the 11 subjects for occipital (O) and frontal (F) lobe. More details in the core of the text.

-	Subject 1	Subject 2	p
O protrusion	R	R	p<0.05
O width	L	R	p>0.05
F protrusion	L	L	p<0.05
F width	L	L	p<0.05

Table 2. **Integrated values for the two SI subjects and p-value (t-test) with H_0: SI subjects belong to the control population.**

SI population: The two SI subjects appear significantly different from the control subjects in the frontal lobes for the left-right component and in the occipital lobes for the antero-posterior component (Fig 6). Right occipital lobes protrude more anteriorly than the left in the two subjects, while it is the opposite in the frontal lobes. The left frontal lobes are also wider than the right counterpart and bend towards it. On the contrary, width measurements are different between the two subjects in the occipital lobes (Table 2). Interestingly, both SI and controls show significant, but opposite, protrusion asymmetries in the occipital lobes.

5. CONCLUSION

Our contributions are threefold. First, we analysed and extended previous works allowing to build a mean shape by using an EM-ICP variant. Second, we showed how the a posteriori probabilities of correspondences (encoded in the match matrices) estimated by the MS-EM-ICP algorithm allow to perform the statistical analysis of bilateral asymmetries. Third, we showed on some real applications that our improved automatic Procrustean mean (and subsequent statistical shape analysis) and our pipeline for asymmetry quantification allow to deal efficiently with large structures. Both methodologies (shape and asymmetry analysis) can deal with numerous applications. In particular, a more practical study comparing the global asymmetry of human and chimpanzee cortex is proposed in another ISBI 2011 paper [13].

An important point of our methodology is that there is no need to define a parametrisation on the surfaces to register, and no assumption on their topology. Moreover, there is no need to have one-to-one correspondences between the surfaces to register, which allows to tackle the difference of sampling and the outliers in an efficient way. As previously mentioned, the process proposed to study analysis can easily be modified to analyse other local patterns such as cortical thickness, curvature, *etc*. Further works will mainly consist in investigating the respective merits of MS2 and MS3 for the estimation of statistical models and comparing them with existing methods [2, 1, 5, 6].

6. REFERENCES

[1] Tobias Heimann, Ivo Wolf, Tomos Williams, and Hans peter Meinzer, "3d active shape models using gradient descent optimization of description length," in *in Proc. IPMI*. 2005, pp. 566–577, Springer.

[2] Stanley Durrleman, Xavier Pennec, Alain Trouvé, and Nicholas Ayache, "Statistical models of sets of curves and surfaces based on currents," in *Medical Image Analysis*, vol. 13, no. 5, pp. 793 – 808, 2009,

[3] Haili Chui, Anand Rangarajan, Jie Zhang, and Christiana Morison Leonard, "Unsupervised learning of an atlas from unlabeled point-sets," in *IEEE Transactions on Pattern Analysis and Machine Intelligence*, vol. 26, pp. 160–172, 2004.

[4] H. Hufnagel, X. Pennec, J. Ehrhardt, N. Ayache, and H. Handels, "Generation of a statistical shape model with probabilistic point correspondences and em-icp," in *IJCARS*, vol. 2, no. 5, pp. 265–273, Mar. 2008.

[5] Fei Wang, Baba C. Vemuri, Anand Rangarajan, and Stephan J. Eisenschenk, "Simultaneous nonrigid registration of multiple point sets and atlas construction," *IEEE Trans. Pattern Anal. Mach. Intell.*, vol. 30, no. 11, pp. 2011–2022, 2008.

[6] Xinyang Liu, Washington Mio, Yonggang Shi, Ivo D. Dinov, Xiuwen Liu, Natasha Lepore, Franco Lepore, Madeleine Fortin, Patrice Voss, Maryse Lassonde, and Paul M. Thompson, "Models of normal variation and local contrasts in hippocampal anatomy," in *MICCAI*, 2008, pp. 407–415.

[7] S. Granger and X. Pennec, "Multi-scale EM-ICP: A fast and robust approach for surface registration," in *ECCV*, 2002, pp. 418–432, Springer.

[8] Benoît Combès and Sylvain Prima, "An efficient EM-ICP algorithm for symmetric consistent non-linear registration of point sets," in *MICCAI*, 2010 594–602, Springer.

[9] Benoît Combès, Robin Hennessy, John Waddington, Neil Roberts, and Sylvain Prima, "Automatic symmetry plane estimation of bilateral objects in point clouds," in *IEEE CVPR*, 1–8, 2008 .

[10] Wei Zeng, Lok Ming Lui, Lin Shi, Defeng Wang, Winnie C. W. Chu, Jack C. Y. Cheng, Jing Hua, Shing-Tung Yau and Xianfeng Gu, "Shape Analysis of Vestibular Systems in Adolescent Idiopathic Scoliosis Using Geodesic Spectra," in MICCAI, 2010, 538–546, Springer.

[11] Fred Spoor, Jean-Jacques Hublin, Marc Braun, and Frans Zonneveld, "The bony labyrinth of Neanderthals," in Journal of Human Evolution*, vol. 44, 2003*.

[12] D. N. Kennedy, K. M. O'Craven, B. S. Ticho, A. M. Goldstein, N. Makris, and J. W. Henson, "Structural and functional brain asymmetries in human situs inversus totalis," *Neurology*, vol. 53, no. 6, pp. 1260–1265, Oct. 1999.

[13] Marc Fournier, Benoît Combès, Neil Roberts, Simon Keller, Tim Crow, William D. Hopkins, and Sylvain Prima, "Surface-based method to evaluate global brain asymmetries:comparison between human and champanzee brains," in *IEEE ISBI*, 2011.

[14] David W. Shattuck, Mubeena Mirza, Vitria Adisetiyo, Cornelius Hojatkashani, Georges Salamon, Katherine L. Narr, Russell A. Poldrack, Robert M. Bilder, and Arthur W. Toga, "Construction of a 3d probabilistic atlas of human cortical structures," *NeuroImage*, vol. 39, no. 3, pp. 1064 – 1080, 2008.